The official journal of the Japan Atherosclerosis Society and
the Asian Pacific Society of Atherosclerosis and Vascular Diseases

Original Article

J Atheroscler Thromb, 2022; 29: 464-473. http://doi.org/10.5551/jat.60509

Three-Dimensional Fluid Dynamical Features of Coronary Plaque Rupture Provoking Acute Coronary Syndrome

Korehito Iida, Takafumi Hiro, Daisuke Fukamachi, Mitsumasa Sudo, Toshihiko Nishida, Naotaka Akutsu, Nobuhiro Murata, Takaaki Kogo, Keisuke Kojima, Takashi Mineki, Takehiro Tamaki, Suguru Migita, Tomoyuki Morikawa and Yasuo Okumura

Division of Cardiology, Department of Medicine, Nihon University School of Medicine, Tokyo, Japan

Aim: Coronary plaque rupture is the main cause of acute coronary syndrome (ACS), but the role of blood flow features around plaque rupture for ACS is still unknown. The present study aimed to assess the relationship between the geometric configuration of ruptured plaque and ACS occurrence using computational fluid dynamics (CFD) by moving particle method in patients with coronary artery disease.

Methods: In this study, 45 patients with coronary artery disease who underwent three-dimensional intravascular ultrasound (IVUS) and had a coronary ruptured plaque (24 plaques with provoked ACS, 21 without) were included. To compare the difference in blood flow profile around ruptured plaque between the patients with and without ACS, the IVUS images were analyzed via the novel CFD analysis.

Results: There were no significant differences in localized flow profile around ruptured plaque between the two groups when the initial particle velocity was 10.0 cm/s corresponded to a higher coronary flow velocity at ventricular diastole. However, when it was 1.0 cm/s corresponded to lower coronary flow velocity at ventricular systole, particles with lower velocity ($0 \leq V \leq 5$ cm/s) were more prevalent around ACS-PR ($p=0.035$), whereas particles with higher velocity ($10 \leq V \leq 20$ cm/s) were more often detected in silent plaque ruptures ($p=0.018$).

Conclusions: Three-dimensional IVUS revealed that coronary plaque rupture was a complex one with a wide variety of its stereoscopic configuration, leading to various patterns of the local coronary flow profile. A novel CFD analysis suggested that the local flow was more stagnant around ACS-provoked ruptures than in silent ones.

Key words: Acute coronary syndrome, Coronary plaque rupture, Three-dimensional intravascular ultrasound, Computational fluid dynamics, Moving particle method

Introduction

Coronary plaque rupture with subsequent thrombosis is the major cause of acute coronary syndrome (ACS)[1]. Nevertheless, all types of coronary plaque rupture do not necessarily lead to provoke ACS, and some types occur silently. Postmortem pathological studies have shown that coronary plaque rupture is likely to occur at the shoulder of eccentric plaque[2]. Recent *in vivo* intravascular ultrasound (IVUS) studies have revealed that the rupture with having subsequent ACS tends to be observed especially at the proximal portion of plaque hill[3, 4] and that multiple plaque ruptures are more common in ACS patients than those with stable angina pectoris[5]. According to the Virchow triad[6], it can be hypothesized that plaque ruptures providing more stagnant blood flow as well as more abundant amounts of subsequent thrombosis more likely provoke ACS, whereas previous studies could not objectively prove this speculation. The reason for this difficulty may be the limitations of observation methods including pathologic studies or *in vivo* intravascular imaging modalities, all of which can only provide transverse or

Address for correspondence: Takafumi Hiro, Division of Cardiology, Department of Medicine, Nihon University School of Medicine, 30-1 Oyaguchi-Kamicho Itabashi-ku, Tokyo 173-8610, Japan E-mail: hiro.takafumi@nihon-u.ac.jp

Received: September 6, 2020 Accepted for publication: January 17, 2021

longitudinal cross-sectional images. Although there is a Doppler guidewire that can measure coronary flow directly within the coronary artery, it can only offer a value of flow velocity just at one point within the coronary lumen. Additionally, animal models have been so far unable to provoke coronary plaque rupture as in human ACS.

Recently, new commercially available technology has been developed, which allows to reconstruct the three-dimensional stereoscopic images of the arterial lumen from a consecutive series of IVUS images (3D-IVUS) and to walk or fly through the arterial lumen on screen with these methods. Thus, the present study aimed to compare the stereoscopic features of plaque rupture between ACS-provoked culprit rupture with the silent rupture in patients who were imaged with IVUS. However, stereoscopic geometry is usually not ready to characterize with a simple objective index. In this study, a newer model of computational fluid dynamics (CFD) called the "moving particle semi-implicit method"[7, 8] was used to identify the specific features of plaque rupture for provoking ACS. This method has some advantages for analyzing blood flow around plaque rupture, when compared with the conventional ways with finite element model, and can provide an objective way to assess the spatial geometry of plaque rupture.

Patients and Methods

Study Patients

This study was a single center observational study for a total of 45 patients (38 men and 7 women) who underwent IVUS for coronary artery disease in our institute and were found to have a distinct coronary plaque rupture by IVUS. The IVUS imaging was performed before percutaneous coronary intervention in all cases. Patients who had advanced kidney disease, hemodialysis, familial hyperlipidemia, severe liver disease, hyperthyroidism, and history of coronary bypass surgery were all excluded. The patients who were not able to show the whole appearance of plaque rupture by IVUS due to severe angulation or calcification and those who did not meet the criteria suitable for CFD analysis described below were also excluded.

When coronary plaque rupture was found in patients with ACS and was considered as the culprit lesion, this rupture was denoted as ACS-provoked plaque rupture (ACS-PR). Whether a rupture of interest was the culprit lesion for ACS or not was determined by the electrocardiographic lead location with ST changes and/or the left ventricular wall regions with echocardiography-derived motion abnormality, whereas there was no other significant stenosis within the same coronary arterial lumen. Conversely, when coronary plaque rupture was not related to the current event as well as the prior event, or when it was found to be a brand new rupture at the follow-up period of percutaneous coronary intervention without any significant cardiovascular event, the rupture was considered to be a silent coronary rupture (Silent-PR).

This study was conducted according to the Declaration of Helsinki and with the approval of the institutional review board (#RK-161108-3). Written informed consent to be investigated was obtained from all of the patients enrolled.

IVUS Imaging

A regular IVUS imaging and its measurements were performed basically according to the expert consensus document on standards for measurements and assessment of IVUS from the Japanese Association of Cardiovascular Intervention and Therapeutics[9]. After administering 1.5 mg isosorbide dinitrate, patients who had rich angiographically detected thrombus in target lesion received thrombus aspiration before IVUS imaging. In angiography, thrombus was considered to be detected when there was a static or mobile mass with distinct characteristics of radio-opacity, which is not a part of plaque thickening. The IVUS transducer was first advanced into the coronary artery as distally as possible. The transducer was then withdrawn during imaging with an automatic motorized pullback system at a speed of 0.5 mm/s. A 40 MHz imaging catheter of the Atlantis™ SR Pro2 (Boston Scientific, Natick, MA, USA) was used during the examinations. Ruptured plaque was defined as a lesion with a distinct cavity that communicated with the lumen accompanied by a residual plaque fragment, an irregular surface, or a tear of the fibrous cap. In the IVUS images, plaque rupture was identified based on the agreement of two independent experienced observers. When the imaged portion was associated with a significant mass of IVUS-derived thrombus on the plaque surface despite thrombus aspiration, such patients were excluded. In IVUS, a relatively homogeneous static or mobile mass with a middle echogenicity, micro-channels, or an echo-scintillation, was diagnosed as thrombus[10].

Three-Dimensional Image Reconstruction

The leading edges of the lumen-intima border as well as the rupture cavity-wall border within the plaque rupture cavity in the IVUS cross-sectional images were consecutively acquired at an interval of 0.2 mm by an automatic pullback device. These

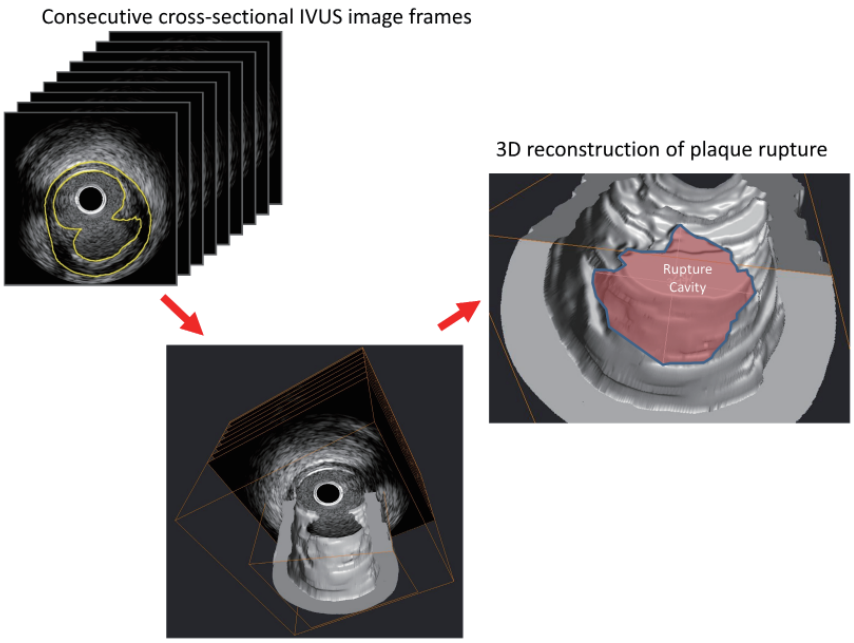

Fig. 1. Three-dimensional reconstruction of IVUS images

Lumen-intimal borders are extracted from consecutive cross-sectional intravascular ultrasound (IVUS) images and are then transferred into a three-dimensional image processing software. Translucent red area corresponds to a rupture cavity space. IVUS, intravascular ultrasound.

images were all semi-automatically traced with a manual adjustment by a commercially available software to edit IVUS image (Echoplaque 3, INDEC Medical Systems Inc., California, USA). The manual adjustment was then meticulously performed via visual inspection, observing neighbor consecutive images back and forth. This tracing was manipulated by two experienced investigators who were unaware of the patient profile. These border-traced slices were then transferred into a three-dimensional image processing program (Avizo Version 5.1.0, FEI Visualization Science Group, Burlington, MA, USA) to reconstruct stereoscopic images of vessel lumen **(Fig. 1)**.

CFD Analysis

A CFD analysis was conducted using a commercially available software (Particleworks, ver 5.1.0, Prometech Software, Tokyo, Japan) that is based on the moving particle semi-implicit method[7, 8]. Conventional CFD methods have usually utilized the finite element model, in which fluid was considered to be a collective structure having a number of meshes and grids. However, the finite element model has some inherent limitations to examine a complex and dynamic flowing fluid, in which computer calculation is often impossible or requires tremendous time. The moving particle semi-implicit method, by contrast, can partly overcome this limitation by considering that fluid is a collection of simple particles such as microspheres. Then, a computer only has to perform a more simplified deterministic calculation solely between the particles to analyze more complex geometry and physics. Thus, the moving particle semi-implicit method was developed for incompressible flow, which is represented by interacting collections of particles **(Fig. 2)**. Governing equations are discretized by a particle interaction model. Compared with the conventional CFD analyses with finite element model, grids are not necessary for any calculation steps. This method can provide numerical values of the three-dimensional velocity vector of all directions for each particle, colorized stereoscopic display of the distribution of particles within a specific range of velocity, and statistical measures of particle flow, which have been difficult to calculate using the finite element method.

In this study, the longitudinal axis of the vessel was taken as the z-axis **(Fig. 3)**. The most proximal side of the ulcerated cavity orifice, which was formed after plaque rupture, was denoted as the origin (zero position) of the z-axis. The area analyzed was selected from the z-axis origin to the portion 8 mm distal to the origin, which was considered to be far enough to evaluate the flow by the CFD model. Therefore, we excluded plaque ruptures that could not provide a full 8-mm-length IVUS image distal to the rupture cavity. Conversely, a 10-mm-length hypothesized cylinder

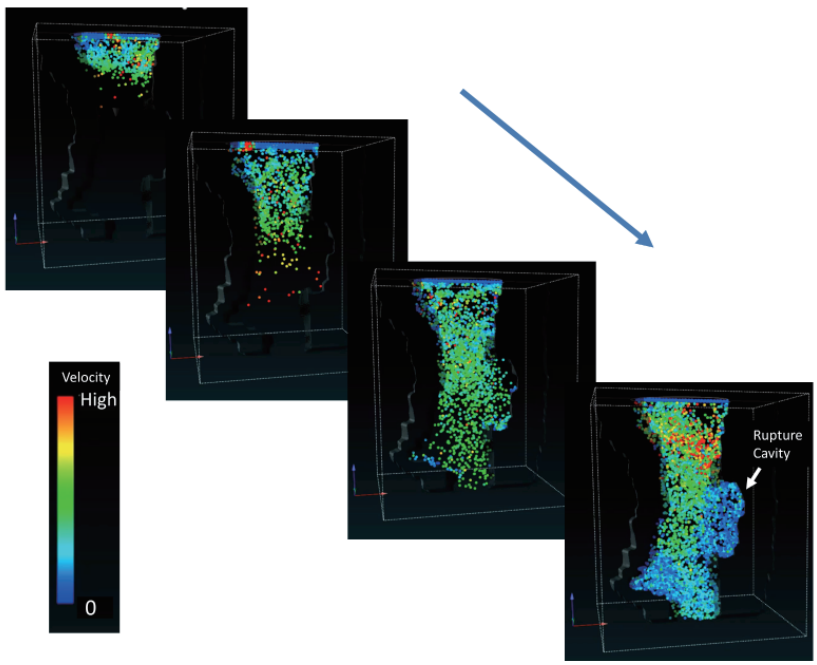

Fig. 2. An example of moving particle semi-implicit CFD analysis

Governing equations are discretized by a particle interaction model. This method can provide numerical values of the three-dimensional velocity vector of all directions for each particle, colorized stereoscopic display of the distribution of particles within a specific range of velocity, and statistical measures of particle flow, which have been difficult to calculate using the finite element method.

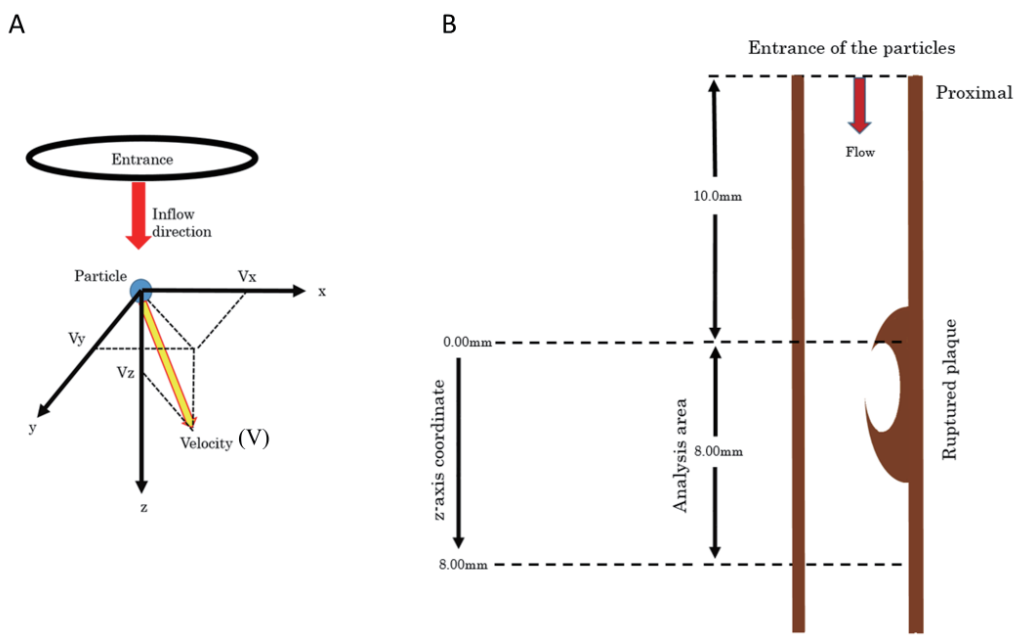

Fig. 3. Definitions of particle velocity vectors and vessel segment for analysis

Three orthogonal axes are defined along the vessel lumen, in which the longitudinal axis of the vessel was taken as the z-axis (Figure 3A). The most proximal side of the ulcerated cavity orifice is denoted as the origin (zero position) of the z-axis. The vessel segment analyzed is selected from the z-axis origin to the portion 8 mm distal to the origin, which is considered to be far enough to evaluate the flow by the computational fluid dynamics (CFD) model (Figure 3B). A 10-mm-length hypothesizes cylinder that has the same cross-sectional shape as the entry of the analyzed area is placed to have a stable supply of particles to the analyzed area.

that had the same cross-sectional shape as the entry of the analyzed area was placed to have a stable supply of particles to the analyzed area.

In this analysis, several assumptions were made as follows:

1) The flow was a constant laminar one.
2) There was no flow resistance at the outlet.
3) There was no flow "slip" on the vessel wall.
4) The particles were not affected by gravity.
5) The blood was incompressible, homogeneous, and Newtonian[11] with a density of 1,050 kg/m^3 and a viscosity of 0.003 PaS[12].
6) The diameter of the particles was 0.1 mm.
7) The distance between the particles was 0.1 mm. Since the analysis area was very small and short in length, we also assumed that the arterial wall was solid.

This analysis also assumed that initial particle velocities were 10.0 and 1.00 cm/s. We chose these two types of initial particle velocity because these velocities approximately corresponded to diastolic and systolic blood flow velocities of the coronary artery, respectively, which were reported in a previous study using Doppler guidewire[13].

The absolute particle velocity (V) was calculated as follows:

$$V=\sqrt{Vx^2+Vy^2+Vz^2},$$

where Vx represents the velocity toward the x axis; Vy, the y axis; and Vz, the z-axis. The lumen area analyzed with a total length of 8 mm, included a plaque rupture, was then divided into 16 slices at an interval of 0.5 mm, and the percent proportion of the number of slow velocity particles ($0 \leq V \leq 5$ cm/s) for each slice was also examined.

Statistical Analysis

Continuous variables were expressed as the mean ± standard deviation. Qualitative data are presented as number (%). Continuous variables with normal distribution were compared by using the Student *t* test, and those without normal distribution were compared by using the Mann–Whitney *U* rank-sum test. Categorical data were compared by using the chi-square test. Statistical analysis was conducted using JMP 9 software (SAS Institute Inc., Cary, NC, USA); *p*-values of <0.05 were considered statistically significant.

Results

Patient Characteristics

Among the 45 patients selected, 24 had a distinct plaque rupture, which was considered to be the culprit for ACS (ACS-PR group), and 21 had a silent plaque rupture (Silent-PR group). These lesions were selected from proximal through middle segments of the left anterior descending artery ($n=21$), the right coronary artery ($n=18$), and the left circumflex coronary artery ($n=8$). In 24 patients of the ACS-PR group, 17 patients had an acute myocardial infarction, one had a recent myocardial infarction, and six had unstable angina pectoris, whereas, in 21 patients of the Silent-PR group, 16 patients had stable angina pectoris, and six had silent myocardial ischemia. In the Silent-PR group, plaque ruptures imaged were not related to any ischemic episodes.

There were no significant differences between patients with ACS-PR and those with Silent-PR in gender (male: 71% vs. 90%, $p=0.100$), age (66 ± 11 vs. 68 ± 8 years, $p=0.602$), body mass index (24.3 ± 2.8 vs. 24.5 ± 4.6, $p=0.870$), and prevalence of hypertension (75% vs. 91%, $p=0.176$), smoking (63% vs. 67%, $p=0.771$), diabetes mellitus (25% vs. 38%, $p=0.344$), and hyperlipidemia (46% vs. 52%, $p=0.661$). The medications at the time of examination, including statin, anti-platelet agents, anti-coagulants, angiotensin-converting enzyme inhibitors, angiotensin receptor blockades, calcium blocker, and beta-receptor antagonists, were all comparable between the groups of ACS-PR and Silent-PR.

Conventional Gray-scale IVUS Findings

The longitudinal diameter of rupture cavity was comparable between the ACS-PR and Silent-PR groups (3.58 ± 1.75 vs. 3.12 ± 1.13 mm, $p=0.625$), although lumen volume within the analyzed portion was significantly smaller in the ACS-PR group (79.3 ± 55.0 vs. 133.0 ± 57.9 mm^3, $p=0.003$), indicating that coronary lumen with ACS-PR was more stenotic (but not clinically significant).

Three-Dimensional Features of Plaque Rupture

Three-dimensional IVUS imaging revealed that there was a wide variety of rupture configuration in the ACS-PR group as well as in the Silent-PR group **(Fig. 4)**. The orifice of plaque rupture was individually shaped with a variety from longitudinal figuration (51%) to oval one (49%) **(Figs. 4A, B)**. The orifice geometry was also determined by the following four patterns in fibrous cap residuals: (1) In some cases, fibrous cap residual was so large that it was called as "fibrous tent" (40%) **(Fig. 4C)**, which has a possibility for disturbing blood flow. (2) When the fibrous cap residuals are located at the distal of rupture orifice, it would become a hazard in coronary luminal blood flow. This pattern was called as "flow-impeding type" (84%) **(Fig. 4D)**. (3) There was a rupture without any fibrous flap (39%) (smoothly flowing type) **(Fig. 4E)**.

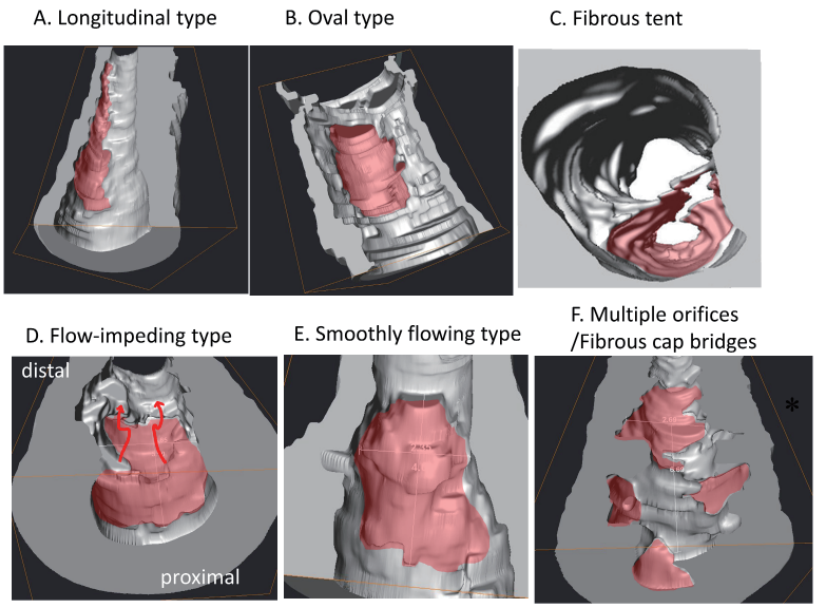

Fig. 4. A variety of cavity configuration of ruptured plaque

(A) Longitudinal orifice. (B) Oval orifice. (C) Fibrous tent (A large tent of fibrous cap residuals over cavity). (D) Flow-impeding type. When the fibrous cap residuals are located at the distal or the side rim of the rupture orifice, it would become a hazard enough to disturb flow directions (like red arrows). (E) Smoothly flowing type, where there was no fibrous flap. (F) Multiple orifices and/or fibrous cap bridges, where fibrous cap residuals formed a "bridge" with a tunnel of rupture cavity having multiple entry/exit orifices. Translucent red area corresponds to a rupture cavity space.

(4) Fibrous cap residuals sometimes formed a "bridge" with a tunnel of rupture cavity having multiple entry/exit orifices (26%) **(Fig. 4F)**. However, since these kinds of rupture cavity configuration were too complex and overlapped each other, it was not readily possible to define these geometric types quantitatively by an objective or numerical index.

Fluid Dynamical Features

When the moving particle semi-implicit CFD was performed through the vessel lumen with plaque rupture, specific features were significantly different between the two groups. At an initial particle velocity of 10.0 cm/s (corresponded to coronary flow velocity during ventricular diastole) **(Fig. 5)**, the averaged absolute velocity of particles was comparable between the ACS-PR and Silent-PR groups (37.1 ± 14.2 vs. 32.1 ± 12.5 cm/s, $p=0.212$). The histogram and the longitudinal profile of particle velocity around the rupture cavity were not significantly different for all particle velocity range. Conversely, at an initial particle velocity of 1.0 cm/s (corresponded to coronary flow velocity during ventricular systole), the averaged velocity of particles was significantly faster in the ACS-PR group than in the Silent-PR group (14.3 ± 6.9 vs. 10.3 ± 6.3 cm/s, $p=0.048$). Furthermore, the histogram of particle velocity was significantly different between the two groups ($p=0.004$), where the ACS-PR group had a wider variety **(Fig. 6A)**. The slow velocity particles ($0 \le V \le 5$ cm/s) were significantly more frequent around the area close to the rupture cavity in the ACS-PR group than in the Silent-PR group ($p=0.035$) **(Fig. 6B)**. The middle -velocity particles ($5 \le V \le 10$ cm/s) were comparably detected around the cavity between the two groups **(Fig. 6C)**. The fast velocity particles ($10 \le V \le 20$ cm/s) were rather significantly more frequent around rupture cavity in the Silent-PR group ($p=0.0184$) **(Fig. 6D)**.

Discussion

The major finding of the present study using the moving particle semi-implicit CFD model was that coronary plaque ruptures with provoking subsequent ACS had specific fluid dynamic features. A wider variety of particle velocity profiles was found around the rupture cavity in the ACS-PR group. Although coronary lumen was significantly more stenotic, and the averaged absolute value of particle velocity was significantly faster in the ACS-PR group, slower velocity particles existed more frequently around rupture cavity in this group than in the Silent-PR group, in which higher velocity particles were rather more frequently observed around the cavity.

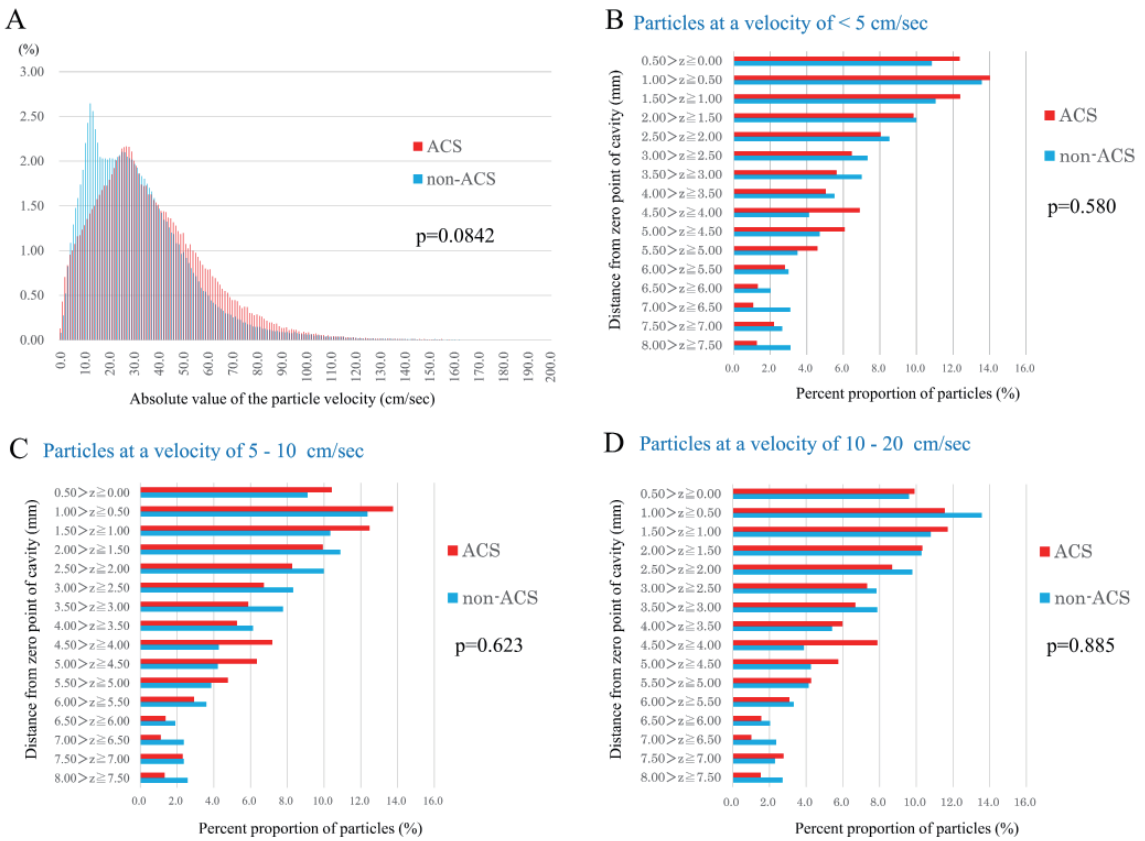

Fig. 5. The results of the CFD analysis at an initial particle velocity of 10.0 cm/s (corresponds to the coronary flow velocity during ventricular diastole)

(A) Histogram of particle velocity around plaque cavity. (B) Percent proportion of particles at a velocity of < 5.0 cm/s. (C) Percent proportion of particles at a velocity of 5.0–10.0 cm/s. (D) Percent proportion of particles at a velocity of 10.0–20.0 cm/s. All graphs are illustrated by incorporating the data of all patients with and without provoking acute coronary syndrome (ACS). Red bars represented the ACS-provoked plaque rupture (ACS-PR) group, and blue bars, the silent plaque rupture (Silent-PR) group. See text for the detail of the results.

Three-Dimensional Configuration of Plaque Rupture

It has been established for a long time that coronary plaque rupture is likely to occur at the shoulder of eccentric plaque[2]. This concept was originally from pathological studies only with viewing cross-sectional vessel slides on a microscope. More recently, longitudinal assessment with intravascular imagings has elucidated that the rupture provoking ACS is more likely to occur at the proximal or middle side of plaque hill[3, 4]. However, the present data suggest that coronary plaque rupture is not a simple geometric phenomenon but rather a more complex one with a wide variety of stereoscopic configuration.

Flow stagnation and ACS

Although plaque rupture is the main cause of ACS, the rupture does not necessarily induce ACS[14, 15]. Previous studies with intravascular imaging modalities have suggested that there are some specific features in ACS-provoked rupture compared with silent rupture[16-18]. IVUS and optical coherence tomography studies have demonstrated that ruptured plaques in the culprit lesions of ACS patients have smaller lumens; greater plaque burdens, area stenosis, and remodeling indices; and more thrombus[16, 17] and that fibrous cap thickness is a critical morphological discriminator of ruptured thin-cap fibroatheroma in patients with ACS[18]. These reports have only demonstrated the surrounding environment or underlying tissue characteristics of ACS-provoked rupture. Our data, however, provided new observations to elucidate the direct geometric and fluid dynamical features of rupture itself as a determinant for provoking ACS.

According to the conventional Virchow triad[6], it could be readily hypothesized that whether a plaque rupture leads to ACS would be determined by how abundant subsequent thrombosis is formed. One of its factors would be how stagnant the blood flow is around the plaque rupture to grow up an obstructive

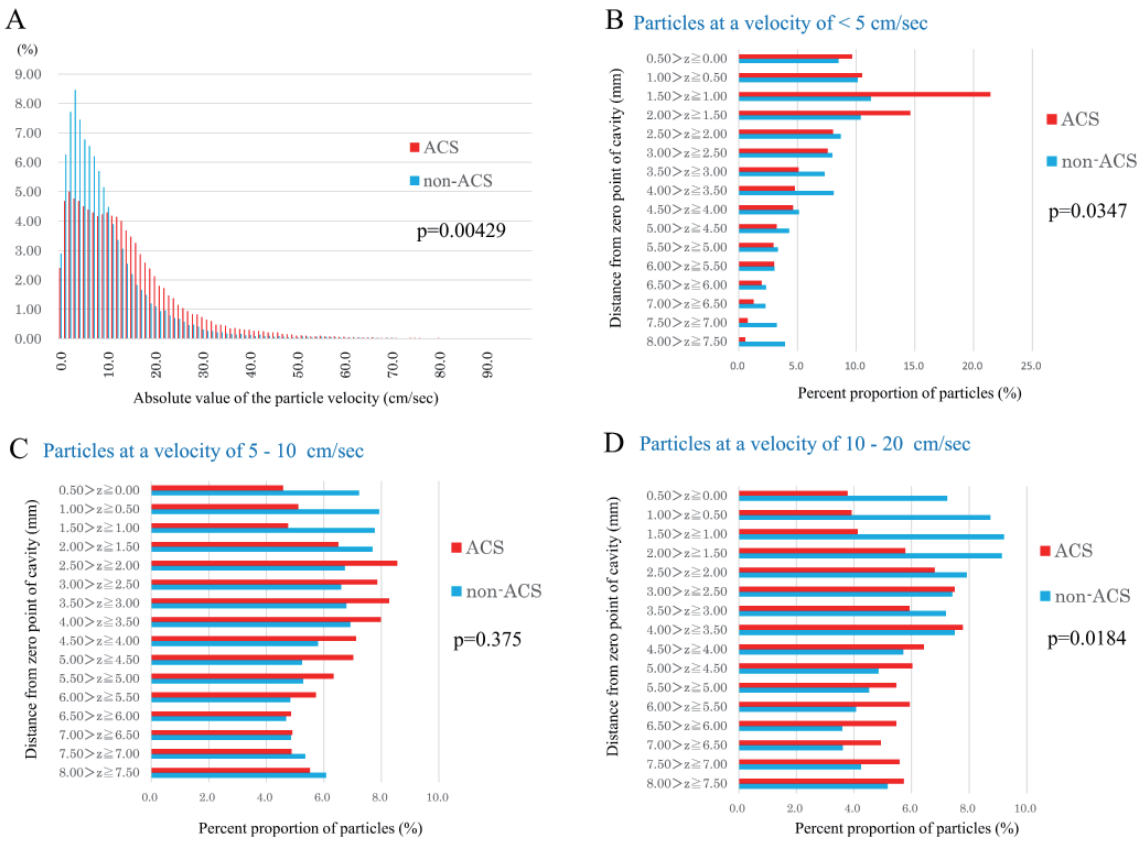

Fig. 6. The results of the CFD analysis at an initial particle velocity of 1.0 cm/s (corresponds to the coronary flow velocity during ventricular systole)

The explanations for this figure are similar to those for Figure 5. See text for the detail of the results.

thrombus[19]. In our data, lumen volume around ruptured plaque was significantly smaller in the ACS-PR group than in the Silent-PR group as shown in previous reports; however, the averaged particle velocity was significantly faster in the ACS-PR group at an initial velocity of 1.0 cm/s. This result was theoretically reasonable when the equation of continuity for incompressible fluid is considered, in which flow velocity is inversely related to cross-sectional area. Faster averaged flow velocity in the ACS-PR group seems to be discrepant from the Virchow triad. We speculate that how large luminal thrombus is formed is not dependent on the averaged flow velocity but rather on more localized flow stagnation. In fact, our data indicated that the slow velocity particles ($0 \leq V \leq 5$ cm/s) were significantly more frequent just around the rupture cavity in the ACS-PR group than in the Silent-PR group. Interestingly, this fact was observed only at an initial velocity of 1.0 cm/s but not at 10.0 cm/s, suggesting that flow stagnation in ventricular systole (slower coronary flow phase) might be more important than ventricular diastole (higher coronary flow phase) for forming ACS-provoking thrombus.

Another interesting finding in the results of our own was that the particle velocity profile had a wider variety in the ACS-PR group. This might suggest that coronary flow around the ruptured cavity was more turbulent in the group. Sumi et al. documented that turbulent flow might promote thrombus formation, which might be a considerable factor to provoke ACS[20].

Mechanism of Flow Stagnation around Plaque Rupture

The variety of flow profile pattern is partly due to the diversity of rupture cavity configuration. The existence of ulcers, flow-disturbing fibrous cap residuals, fibrous cap bridges or tents, or multiple entry/exit rupture, which were all observed in the present study, might be all related to the occurrence of flow stagnation or turbulence around the rupture cavity. From a complex mixture of these factors, some plaque rupture in some patients would have a

significant flow stagnation to cause ACS. It was documented that plaque ruptures at the proximal side of plaque hill more frequently provoke ACS than that at the other portions[4]. Such proximal plaque ruptures may be frequently associated with fibrous cap residual at the distal end of the rupture cavity, which in turn disturbs blood flow.

The diversity of rupture geometry can be theoretically explained partly by fracture mechanics[21]. According to these mechanics, the fracture of material is classified into two categories: brittle and ductile fractures. In brittle fracture, the material is broken down by cleavage without any apparent plastic deformation, whereas extending plastic deformation occurs in ductile fracture. It might be speculated that fibrous cap fracture is ductile and that lipid-core breakdown is a brittle feature, since fibrous components can be easily extensive, but lipidic or necrotic cores are just a collection of fluids or solid granules[2, 22]. In addition, fractures of material are usually expanded, selecting the most fragile point around the ruptured area. Actually, plaque tissue structure is inhomogeneous, filled with fibrous, lipidic, and/or necrotic materials in a very complex fashion, in which there are significant individual differences. Furthermore, degrees of inflammation or inflammatory cell accumulation are also very different among plaques, which would yield complex heterogeneity in weakness within the plaque wall[23, 24]. Therefore, plaque rupture is inherently having various degrading processes interacting with each other within a single plaque, and it should be stressed here that plaque rupture is not a simple geometric phenomenon but rather a very intricate one with a wide variety among lesions or patients.

Study Limitations

Several study limitations should be considered. First, this was a retrospective analysis in a single center, having various limitations for the generalization of our results shown below. Second, the number of patients was relatively small due to strict criteria for performing the CFD analysis. Third, to perform the CFD analysis as realistic as possible, we chose relatively straight coronary segments of the lumen into which the IVUS catheter could be inserted with minimal bending. However, the use of three-dimensional IVUS images still has the potential for errors in reconstructing the lumen contour. Fourth, the CFD analysis used several initial assumptions, such as using a constant laminar flow with noncompressible, homogeneous, and Newtonian blood, no flow resistance at the outlet, no flow slip on the vessel wall, no gravity considered, and solid vessel wall, for the purpose of simplified calculations. However, the assumptions used in this study have been widely accepted in previous papers as allowable for the assessment of the biomechanical properties of atherosclerotic lesions. Moreover, it might be speculated that this method would be useful not only to analyze local flow dynamics around plaque rupture but also to predict whether a plaque rupture shape could provoke ACS. Additionally, the coagulability of blood around the plaque rupture was not considered in the present study, which is also an important component of the Virchow triad. A more comprehensive assessment of thrombus formation around plaque rupture would be warranted in the future.

Conclusions

Three-dimensional IVUS revealed that coronary plaque rupture was a complex one with a wide variety of its stereoscopic configuration, leading to various patterns of the local coronary flow profile. A novel way of CFD analysis with moving particle method suggested that the slow velocity particles at ventricular systole were significantly more frequent around the area close to the rupture cavity in the ACS-PR group than in silent ones and that, in other words, the local flow was more stagnant around the ACS-PR group. Additionally, it suggested that the distribution of blood flow velocity at ventricular systole was wider in the ACS-PR group.

Acknowledgements

This work was partly supported by a Grant-in-Aid for Scientific Research (JSPS KAKENHI Grant Number 16K09481) of the Ministry of Education, Japan.

Conflict of Interest

Dr. Hiro and Dr. Okumura worked at the endowed department at Nihon University School of Medicine donated by Boston-Scientific Japan Co. Ltd, a manufacturer of IVUS machine used in the present study. The remaining authors have nothing to disclose.

References

1) Fuster V, Stein B, Ambrose JA, Badimon L, Badimon JJ, Chesebro JH: Atherosclerotic plaque rupture and thrombosis. Evolving concepts. Circulation, 1990; 82: II47-59
2) Richardson PD, Davies MJ, Born GV: Influence of plaque configuration and stress distribution on fissuring

of coronary atherosclerotic plaques. Lancet, 1989; 2: 941-944
3) Fukumoto Y, Hiro T, Fujii T, Hashimoto G, Fujimura T, Yamada J, Okamura T, Matsuzaki M: Localized elevation of shear stress is related to coronary plaque rupture: a 3-dimensional intravascular ultrasound study with in-vivo color mapping of shear stress distribution. J Am Coll Cardiol, 2008; 51: 645-650
4) Tanaka A, Shimada K, Namba M, Sakamoto T, Nakamura Y, Nishida Y, Yoshikawa J, Akasaka T: Relationship between longitudinal morphology of ruptured plaques and TIMI flow grade in acute coronary syndrome: a three-dimensional intravascular ultrasound imaging study. Eur Heart J, 2008; 29: 38-44
5) Hong MK, Mintz GS, Lee CW, Lee BK, Bong-Ki Lee, Yang TH, Kim YH, Song JM, Han KH, Kang DH, Cheong SS, Song JK, Kim JJ, Park SW, Park SJ: The site of plaque rupture in native coronary arteries: a three-vessel intravascular ultrasound analysis. J Am Coll Cardiol, 2005; 46: 261-265
6) Virchow R: Phlogose and thrombose in gerasystem. In: Virchow R (editor): Gesammelte Abhandlungen zur Wissenchaftichen Medicin. Frankfurt: Von Meidinger Sohn, 1856: 458-636
7) Koshizuka S, Tamako H, Oka Y: A particle method for incompressible viscous flow with fluid fragmentation. Comput Fluid Dyn J, 1995; 4: 29-46
8) Koshizuka S, Oka Y: Moving-particle semi-implicit method for fragmentation of incompressible fluid. Nucl Sci Eng, 1995; 123: 421-434
9) Saito Y, Kobayashi Y, Fujii K: Clinical expert consensus document on standards for measurements and assessment of intravascular ultrasound from the Japanese Association of Cardiovascular Intervention and Therapeutics. Cardiovasc Interv Ther, 2020; 35: 1-12
10) Chemarin-Alibelli MJ, Pieraggi MT, Elbaz M, D Carrié, Fourcade J, Puel J, Tobis J: Identification of coronary thrombus after myocardial infarction by intracoronary ultrasound compared with histology of tissues sampled by atherectomy. Am J Cardiol, 1996; 77: 344-349
11) Friedman MH, Bargeron CB, Duncan DD, Hutchins GM, Mark FF: Effects of arterial compliance and non-Newtonian rheology on correlations between intimal thickness and wall shear. J Biomech Eng, 1992; 114: 317-320
12) Krijger JK, Heethaar RM, Hillen B, Hoogstraten HW, Ravensbergen J: Computation of steady three-dimensional flow in a model of the basilar artery. J Biomech, 1992; 25: 1451-1465
13) Hozumi T, Yoshida K, Akasaka T, Asami Y, Ogata Y, Takagi T, Kaji S, Kawamoto T, Ueda Y, Morioka S: Noninvasive assessment of coronary flow velocity and coronary flow velocity reserve in the left anterior descending coronary artery by Doppler echocardiography: comparison with invasive technique. J Am Coll Cardiol, 1998; 32: 1251-1259
14) Davies MJ, Bland JM, Hangartner JR, Angelini A, Thomas AC: Factors influencing the presence or absence of acute coronary artery thrombi in sudden ischaemic death. Eur Heart J, 1989; 10: 203-208
15) Goldstein JA, Demetriou D, Grines CL, Pica M, Shoukfeh M, O'Neill WW: Multiple complex coronary plaques in patients with acute myocardial infarction. The N Engl J Med, 2000; 343: 915-922
16) Kotani J, Mintz GS, Castagna MT, Pinnow E, Berzingi CO, Bui AB, Pichard AD, Satler LF, Suddath WO, Waksman R, Laird JR Jr, Kent KM, Weissman NJ: Intravascular ultrasound analysis of infarct-related and non-infarct-related arteries in patients who presented with an acute myocardial infarction. Circulation, 2003; 107: 2889-2893
17) Fujii K, Kobayashi Y, Mintz GS, Takebayashi H, Dangas G, Moussa I, Mehran R, Lansky AJ, Kreps E, Collins M, Colombo A, Stone GW, Leon MB, Moses JW: Intravascular ultrasound assessment of ulcerated ruptured plaques: a comparison of culprit and nonculprit lesions of patients with acute coronary syndromes and lesions in patients without acute coronary syndromes. Circulation, 2003; 108: 2473-2478
18) Tian J, Ren X, Vergallo R, Xing L, Yu H, Jia H, Soeda T, McNulty I, Hu S, Lee H, Yu B, Jang IK: Distinct Morphological Features of Ruptured Culprit Plaque for Acute Coronary Events Compared to those with Silent Rupture and Thin-Cap Fibroatheroma: a Combined Optical Coherence Tomography and Intravascular Ultrasound Study. J Am Coll Cardiol, 2014; 63: 2209-2216
19) Yamashita A, Furukoji E, Marutsuka K, Hatakeyama K, Yamamoto H, Tamura S, Ikeda Y, Sumiyoshi A, Asada Y: Increased vascular wall thrombogenicity combined with reduced blood flow promotes occlusive thrombus formation in rabbit femoral artery. Arterioscler Thromb Vasc Biol, 2004; 24: 2420-2424
20) Sumi T, Yamashita A, Matsuda S, Goto S, Nishihira K, Furukoji E, Sugimura H, Kawahara H, Imamura T, Kitamura K, Tamura S, Asada Y: Disturbed blood flow induces erosive injury to smooth muscle cell-rich neointima and promotes thrombus formation in rabbit femoral arteries. J Thromb Haemost, 2010; 8 : 1394-1402
21) Anderson TL: Fracture mechanics: fundamentals and applications. 3rd ed Boca Raton, FL: Taylor & Francis, 2005
22) Vengrenyuk Y, Carlier S, Xanthos S, Cardoso L, Ganatos P, Virmani R, Einav S, Gilchrist L, Weinbaum S: A hypothesis for vulnerable plaque rupture due to stress-induced debonding around cellular microcalcifications in thin fibrous caps. Proc Natl Acad Sci U S A, 2006; 103: 14678-14683
23) Davies MJ, Woolf N, Rowles P, Richardson PD: Lipid and cellular constituents of unstable human aortic plaques. Basic Res Cardiol, 1994; 89 Suppl 1: 33-39
24) Lendon CL, Davies MJ, Born GV, Richardson PD: Atherosclerotic plaque caps are locally weakened when macrophages density is increased. Atherosclerosis, 1991; 87: 87-90